Murine models for triple-negative breast cancer with differential responsiveness to immunotherapy

Thomas J Kalantzakos,[1] Yufan Zhou,[1] Xingyu Liu,[1] Joshua Proehl,[1] Cameron Durfee,[1] Ian Tamayo[1], Nuri Alpay Temiz,[2,3] Benjamin Troness,[1] Anusha Soni,[1] Harshita B Gupta,[1,#] & Reuben S Harris[1,4,#]

[1]Department of Biochemistry and Structural Biology, Long School of Medicine, University of Texas Health San Antonio, San Antonio, Texas, USA; [2]Institute for Health Informatics, University of Minnesota, Minneapolis, Minnesota, USA; [3]Masonic Cancer Center, University of Minnesota, Minneapolis, Minnesota, USA; [4]Howard Hughes Medical Institute, University of Texas Health San Antonio, San Antonio, Texas, USA

[#]Correspondence: GuptaH@uthscsa.edu or rsh@uthscsa.edu

ABSTRACT

Breast cancer is the most common cancer diagnosis in women. Clinical studies with triple-negative breast cancer (TNBC) are encouraging for immunotherapy combined with chemotherapy (anti-PD-1 with paclitaxel and/or carboplatin). However, additional clinical advances may be pursued more rapidly with assistance from preclinical TNBC models including syngeneic mammary tumor cell lines. Here, we report two mammary tumor cell lines that exhibit differential responsiveness to immunotherapy *in vivo*. Spontaneous mammary tumors from C57BL/6J MMTV-Cre Trp53$^{fl/+}$ animals were passaged serially in cell culture and *in vivo* in the mammary fat pad of fully wildtype animals. The resulting lines, MM001i and MM008i, lost *Trp53* and formed 1000 mm^3 tumors in the mammary fat pad within 21-28 days. Despite originating from the same genetic background, these lines exhibit differential responses to immunotherapy. For anti-PD-1 therapy, MM001i is poorly responsive and MM008i is strongly responsive with near-complete tumor regression. In comparison, both MM001i and MM008i respond rapidly to anti-CTLA-4 therapy. Both models express unique tumor antigens as evidenced by immunity to subsequent engraftments. Primary MM008i tumors exhibit greater T cell infiltration, and CD8-positive T lymphocytes are required for anti-PD-1 responses. These TNBC models are promising for further mechanistic studies and testing future single and combinatorial therapies.

KEYWORDS: anti-tumor immune responses; checkpoint therapy; immunotherapy; syngeneic murine tumor models; triple-negative breast cancer (TNBC)

39 ## Introduction

40 Breast cancer is the most commonly diagnosed malignancy worldwide and a leading
41 cause of cancer-related death in women.[1, 2] Clinically, breast cancer is characterized based on
42 expression of estrogen receptor (ER), progesterone receptor (PR), and/or human epidermal
43 growth factor receptor 2 (HER2). Triple negative breast cancer (TNBC) lacks expression of these
44 three markers, accounts for 15-20% of breast cancer diagnoses, and is associated with poor
45 clinical outcomes.[3] For example, 30-40% of TNBC patients exhibit tumor recurrence within 3-5
46 years of the initial diagnosis and treatment.[4, 5] The most common genetic defect in TNBC is
47 mutation of *TP53* (hereafter *p53*) in 75-80% of cases,[6, 7] with most tumors incurring full loss-of-
48 function alleles.[8] TNBC tumors are highly heterogeneous and often subdivided into six molecular
49 clusters: basal-like 1, basal-like 2, immunomodulatory, mesenchymal, mesenchymal stem-like,
50 and luminal androgen receptor subtypes.[9]

51 Several clinical trials have demonstrated the benefit of immunotherapy approaches in
52 TNBC, particularly through monoclonal antibody (mAb) targeting of programmed cell death
53 protein 1 (PD-1) and cytotoxic T-lymphocyte antigen 4 (CTLA-4). The efficacy of immunotherapy,
54 particularly anti-PD-1 antibody therapy (αPD-1), in combination with chemotherapy, is becoming
55 established in both primary and metastatic TNBC settings. In the KEYNOTE-522 clinical trial,
56 adding αPD-1 to neoadjuvant chemotherapy (paclitaxel and carboplatin followed by
57 doxorubicin/epirubicin and cyclophosphamide) in early TNBC improved pathological complete
58 response from 51% to 65%.[10] Further, the KEYNOTE-355 trial, conducted on advanced TNBC
59 patients, demonstrated a robust increase in overall survival when combining αPD-1 and
60 chemotherapy in patients with high programmed cell death-ligand 1 (PD-L1) expression.[11]
61 Emerging studies are also evaluating combination immunotherapy approaches. For example, the
62 BELLINI trial is investigating dual inhibition of PD-1 and CTLA-4, showing signs of efficacy in
63 early-stage TNBC.[12] Additionally, bi-specific antibodies targeting PD-1 and CTLA-4 combined with

64 paclitaxel have shown survival benefits for TNBC patients in the metastatic setting.[13] Additional
65 trials are ongoing that combine immunotherapies with radiation therapy and/or chemotherapy
66 (*e.g.*, NCT04683679, NCT05491226, NCT06472583). However, despite these recent advances,
67 a large subset of TNBC patients still suffers from disease progression, which warrants further
68 mechanistic and therapeutic studies.

69 Syngeneic murine models are useful for preclinical evaluation of candidate therapeutics
70 *in vivo.* To date, only a few murine syngeneic models for TNBC have been reported. The first,
71 E0771, was derived in 1955 from a spontaneously occurring breast adenocarcinoma in a C57BL/6
72 background.[14] Treatment of this model with αPD-1 leads to partial tumor regression[15] and
73 enhanced efficacy when combined with other agents.[16] αPD-1 and αCTLA-4 therapies also
74 associate with increases in circulating $CD8^+$ T lymphocytes in this model.[16, 17] However, it is an
75 older model and reports conflict on several key properties including genotype and hormone
76 receptor status.[18-20] Another commonly used line is 4T1, isolated from a metastatic tumor in a
77 BALB/c animal.[21] However, this line is poorly responsive to immunotherapy due at least in part to
78 a Th2-biased immune response.[22, 23] Other models, such as PyMT,[24] AT-3,[25] and WT145[26] are
79 additionally complicated by viral transgenes and/or chemical exposures.

80 Here, we report the development of two new cell lines, MM001-immunoconditioned
81 (MM001i) and MM008i, derived from mammary tumors that arose on C57BL/6J background.
82 Briefly, the primary mammary tissues were engineered to be heterozygous for *p53*, but the second
83 copy was lost during tumor development in both cell lines. Serial passage in culture and *in vivo*
84 resulted in MM001i and MM008i, which form 1000 mm^3 tumors approximately 21-28 days after
85 engraftment. Both lines are negative for ER, PR, and HER2 (triple-negative) and provoke anti-
86 tumor immune responses, as evidenced by immune memory formation and acquired resistance
87 to additional challenge by the same tumor cell line. Both lines also respond to αCTLA-4
88 immunotherapy, but only MM008i responds to αPD-1 immunotherapy. This differential

89 responsiveness is dependent on $CD8^+$ T lymphocytes and may be attributable to improved
90 immune cell infiltration in MM008i tumors ($CD45^+$ immune cells, $CD8^+$ T lymphocytes). Taken
91 together, these syngeneic tumor lines constitute new models for TNBC and provide a foundation
92 for additional studies on molecular mechanisms and responsiveness of different
93 immunotherapies.
94

95 ## Materials and Methods

96 ### Mouse care

97 All animal studies were approved by the University of Texas Health San Antonio (UT
98 Health) Institutional Animal Care and Use Committee (IACUC Protocol ID: 20220056AR) and
99 conducted in accordance with ARRIVE guidelines 2.0.[27] The study period was 2023-2025. "Guide
100 for the care and use of laboratory animals" guidelines were followed, and the study adhered to
101 the principles of 3Rs (Replace, Reduce, and Refine). The Lab Animal Resources (LAR) facilities
102 at UT Health are AAALAC (accredited unit: #000341) and USDA (registration number: 74-R-0071)
103 approved. 24/7/365 LAR staff include veterinarians, facility staff, and animal technicians for
104 services including complete husbandry, routine monitoring, examination of mice health and
105 supportive care. 3-5 animals per cage were housed in specific pathogen-free conditions
106 maintained at 22°C under a standard 12-hour light/dark cycle and given food and water *ad libitum*.
107 Initial breeder pairs for WT (Jax strain 000664) and NOD.Cg-Prkdc^{scid}Il2rg^{tm1Wj1}/SzJ [nonobese
108 diabetic/severe combined immunodeficiency (NOD/SCID)/IL2Rγ KO, NSG, Jax strain 005557]
109 mice were purchased from Jackson Laboratory (Bar Harbor, ME, USA) and then propagated in-
110 house. NSG mice were maintained under sterile conditions. 8-10 weeks-old mice were enrolled
111 for tumor studies. All immunocompetent mice were on C57BL/6J background, and only females
112 were used for mammary tumor experiments.

113 Mice were checked one day post-injection, and then twice a week for tumor growth,
114 morbidity, weight loss, and dehydration. Mice were euthanized if they were in distress, lost >20%

115 body weight, showed a body score <2, and/or reached experimental end points such as 1000
116 mm^3 tumor volumes. The signs of distress included but were not limited to dehydration, cachexia,
117 weakness, ruffled body fur, or hunched back. Euthanasia was done as recommended by the
118 American Veterinary Medical Association guidelines for the Euthanasia of Animals. Briefly, mice
119 were subjected to inhalation of 99% pure CO_2 with a fill rate of 30-70% chamber volume/minute
120 for 2 minutes followed by cervical dislocation. Anesthesia was not used for the experiments
121 performed for this study.
122

123 **Tumor harvesting from mice**

124 *MMTV-Cre p53*$^{fl/+}$ mice were bred initially at the University of Minnesota and subsequently
125 at UT Health prior to the present studies. Genotypes were confirmed via PCR[28] using primers:
126 1F: 5'-TAACACTCTTGGGATGCTGAG-3', 10F: 5'-AAGGGGTATGAGGGACAAGG-3', and 10R: 5'-
127 GAAGACAGAAAAGGGGAGGG-3'. Spontaneously arising primary mammary tumors in these
128 mice were extracted under sterile conditions, and single-cell suspensions were made by tumor
129 dissection and mechanical dissociation. Cells were transferred to a cell culture flask in RPMI-
130 1640 (Thermo Fisher Scientific, Waltham, MA, USA) supplemented with 10% fetal bovine serum
131 (FBS, Thermo Fisher Scientific) and 1% penicillin-streptomycin (complete medium, Thermo
132 Fisher Scientific), under standard culturing conditions (37°C, 5% CO_2). Once the cells reached
133 80% confluence, cells were harvested by 0.05% trypsin-EDTA (Gibco, Thermo Fisher Scientific)
134 for engraftment into mice. Freeze downs were made simultaneously in 90% FBS/10% DMSO
135 (Sigma-Aldrich, St. Louis, MO, USA). All cell lines were confirmed to be free of mycoplasma
136 contamination by detection kit (catalog no. LT07-318, Lonza Bioscience, Walkersville, MD, USA)
137 prior to freezing or experimental use. Cultured cells in passage 3 or 4 were used for subsequent
138 characterization and engraftment studies, which we have found yield reproducible results across
139 multiple biological replicates.

140

141 **Serial passage to develop conditioned cell lines**

142 Cells were trypsinized, washed with endotoxin-free, sterile phosphate-buffered saline
143 (PBS) and combined at 1:1 ratio with Cultrex Basement Membrane Extract, PathClear (R&D
144 Systems, Minneapolis, MN, USA) for a final cell count as indicated (2.5 or 5 x 10^6 cells) in a final
145 volume of 100 µL per injection. Cells were injected subcutaneously or into the 4th inguinal
146 mammary fat pads of mice. Initial engraftments were conducted in both WT and NSG mice. As
147 tumors successfully engrafted in both strains, subsequent engraftments for serial passage were
148 conducted in WT mice alone. At day 7, tumors were measured using Vernier caliper (Thermo
149 Fisher Scientific) and then monitored twice a week until reaching a volume of 1000 mm^3 using the
150 equation $V=0.5 \times L \times W^2$.[29] Tumors reaching 1000 mm^3 were subsequently isolated post-humane
151 mouse euthanasia. The process was repeated for at least two rounds per cell line.

152

153 **Flow cytometry**

154 MM001i or MM008i cells were plated overnight in 6-well plates in complete medium (3 x
155 10^5 cells/well). Cells were then incubated with fresh complete medium supplemented with either
156 vehicle or interferon-gamma (IFN-γ) (R&D Systems) for 24 hours. Cells were harvested and
157 counted using the Countess cell counter (Thermo Fisher Scientific). 1 x 10^6 cells per condition
158 were analyzed for subsequent steps. Cells were washed with PBS, stained for live/dead dye
159 (Zombie Yellow Fixable Viability dye) in PBS for 40 min at 4°C in the dark. Cells were washed in
160 1x PBS and incubated with anti-CD16/32 (BioLegend, San Diego, CA, USA) in flow buffer (PBS
161 + 2% FBS) to prevent non-specific antibody binding for 30 minutes at 4°C, followed by incubation
162 with anti-mouse PD-L1 (PE, clone 10F.9G2), H-2KB (Pacific Blue, clone AF6-88.5), or matched
163 isotype controls (BioLegend). Cells were fixed in 0.4% buffered formalin. Cells were acquired
164 using BD LSRFortessa (BD Biosciences, San Juan, CA, USA) and analyzed using FACSDiva and
165 FlowJo 10.10.0 (BD Biosciences). Positivity thresholds were determined based on isotype control

166 staining.

167

168 **Immunotherapy experiments**

169 2.5 x 10^6 MM001i or MM008i cells were suspended in 50 µL endotoxin-free PBS. An equal
170 volume of basement membrane was added to reach a final volume of 100 µL/injection. For all
171 immunotherapy experiments, mice were randomized manually to equalize numbers across
172 treatment groups. Mice with no palpable tumor by day 7 (tumor vol < 200 mm^3) were excluded
173 due to likely failed injection (<25% of injections). Each mouse received two injections (one per
174 inguinal mammary fat pad), and the sample size for each group was based on the total number
175 of animals enrolled for each condition. On day 7, an initial tumor measurement was taken as
176 previously described. Tumors were monitored twice a week, and the mice were euthanized when
177 tumors reached 1000 mm^3, or when they displayed signs of distress. 7 days post-injection, each
178 mouse received an intraperitoneal (i.p.) injection of 100 µg of αPD-1 (catalog no. BE0146, clone
179 RMP1-14, BioXCell NH, USA), αCTLA-4 (catalog no. BE0131, clone 9H10, BioXCell), a
180 combination of the two, or their respective isotype controls (catalog # BE0089 and BE0087,
181 BioXCell). Mice injected with MM001i received two additional treatments on days 12 and 19.

182

183 **Memory response experiments**

184 WT mice with complete tumor regression in response to immunotherapy were enrolled in
185 memory rechallenge experiments. For MM001i, this consisted of one mouse previously treated
186 with αPD-1 and four that received αCTLA-4 or a combination of αPD-1 and αCTLA-4. Additionally,
187 five animals were enrolled that completely cleared MM008i tumors from each treatment group. 90
188 days after the last tumor evaluation, mice were reinjected with 2.5 x 10^6 cells of the initial cell line
189 at the same inguinal mammary fat pad. No further treatments were administered. Tumors were
190 measured beginning 7 days post-injection and monitored as above until the endpoint was

191 reached. The control group consisted of age-matched, naïve, previously unchallenged WT mice
192 injected with the same tumor cell line as the rechallenge group but not treated with any
193 immunotherapy agent.
194
195 **Immunohistochemistry**
196 IHC was performed as previously described.[30] In brief, FFPE tissues and cell pellets were
197 sectioned at 4 μm and mounted on positively charged glass slides. The slides were deparaffinized
198 at 65°C for 20 minutes, rehydrated with three 5-minute washes in CitriSolv (Decon Labs,
199 Swedeland, Pennsylvania, USA) followed by 3-minute washes in graded ethanol to 80%, and
200 finished with a 5-minute wash in running water. Antigen retrieval was performed in 1x Reveal
201 Decloaker (Biocare Medical, Pacheco, California, USA) by steaming for 35 minutes and returned
202 to room temperature with 30 minutes off the steamer. The slides were washed for 5 minutes in
203 running water and then in tris-buffered saline with 0.1% tween (TBST, Thermo Fisher Scientific).
204 Endogenous peroxidase activity was suppressed by soaking slides in 3% H_2O_2 diluted in TBST
205 for 10 minutes, followed by a 5-minute wash in running water. The slides were soaked in
206 Background Sniper (Biocare Medical) for 15 minutes, immediately followed by overnight
207 incubation of primary antibody diluted using 10% Sniper in TBST at 4°C. The following primary
208 antibodies were used: αER (Catalog no. AB32063, 1:2000, Abcam, Cambridge, UK), αPR
209 (Catalog no. 25871-AP-1, 1:10000, ProteinTech, Rosemont, Illinois, USA), αHER2 (Catalog no.
210 CST2165S, 1:1000, Cell Signaling Technologies, Danvers, Massachusetts, USA), αCD3 (Catalog
211 no. AB135372, 1:250, Abcam), αCD8 (Catalog no. AB209775, 1:600, Abcam) and αCD19
212 (Catalog no. AB317335, 1:600, Abcam). After overnight incubation, the slides were brought to
213 room temperature and washed in TBST for 5 minutes. Next, they were incubated with Novolink
214 Polymer (Lieca Biosystems, Deer Park, Illinois, USA) for 30 minutes and developed using
215 Novolink DAB substrate kit (Lieca Biosystems) for 5 minutes. Slides were immediately washed in

216 running water to quench substrate development and counterstained for 10 minutes using Mayer's
217 hematoxylin solution (Electron Microscopy Sciences, Hatfield, Pennsylvania, USA). Slides were
218 then dehydrated in degraded alcohols and CitriSolv and then cover-slipped using Permount
219 mounting media (Fisher Scientific).
220

221 **Immune cell infiltration analysis by IHC**

222 MM001i and MM008i sections were used to assess the infiltration of T and B lymphocytes
223 in n=4-5 tumors. T cells and B cells were visualized using αCD3 and αCD19 antibodies
224 respectively, as described above. T cell and B cell densities were calculated using QuPath v0.5.1
225 bioimage analysis software using the positive cell detection algorithm. 5 random uniform regions
226 of interest (ROIs) were selected within each tumor section and cell density was averaged for all
227 ROIs per tumor.
228

229 **Immune cell infiltration analysis by flow cytometry**

230 Mice were euthanized, and tumors were harvested once the mean group volume reached
231 750 mm^3. Tumors were digested, and single-cell suspensions were made using 0.3 mg Liberase
232 (Thermo Fisher Scientific) and 0.2 mg DNase I (Sigma-Aldrich) per tumor in incomplete RPMI-
233 1640. Tumors were mechanically dissociated, minced and incubated with shaking at 37°C for 30
234 minutes. Cell suspensions were harvested, passed through 70 μM strainers, and counted. 5×10^6
235 cells were stained for surface markers as above. Cells were incubated with αCD16/32 to prevent
236 non-specific antibody binding as above, followed by staining with αCD45 (FITC), αCD3 (PE-Cy7),
237 αCD8 (APC-Cy7), αCD4 (Bv786), αCD62L (Bv711), αPD-1 (PerCP-Cy5), αCD44 (Pacific Blue),
238 αTIM3 (APC), or αGr1 (Bv786), αCD86 (APC-Cy7), αCD11c (PE), αCD11b (PerCP-Cy5), αB220
239 (AF700), αNK1.1 (APC) post live/dead staining (Zombie Yellow Fixable Viability dye). All
240 antibodies and Zombie Yellow Fixable Viability dye were purchased from BioLegend. Cells were

241 washed, fixed in 0.4% buffered formalin, and analyzed as mentioned above.

242

243 **$CD8^+$ neutralization experiments**

244 2.5 x 10^6 MM008i cells were injected into the mammary fat pads of immunocompetent WT
245 mice as previously described. On day 6, initial tumor measurements were taken, and mice were
246 randomized into groups. On days 6, 9, and 12, each mouse received an i.p. injection of 200 µg of
247 αCD8 antibody (catalog no. BE0004-1, clone 53-6.7, BioXCell) or its isotype control (catalog no.
248 BE0089, clone 2A3, BioXCell). On day 7, each mouse received a single i.p. injection of 100 µg of
249 αPD-1 or its isotype control, as previously described. Tumors were measured biweekly, and mice
250 were euthanized at day 25 or when tumor volumes reached 1000 mm^3. At day 13 and before
251 complete tumor regression, a small subset of tumors representing each treatment group were
252 isolated to assess immune infiltration of $CD8^+$ T lymphocytes by immunohistochemistry.

253

254 **Bulk RNA-sequencing of MM001i and MM008i cell lines and tumors**

255 RNA from two biological replicates each of MM001i and MM008i grown in culture were
256 isolated using the Qiagen RNeasy Mini Kit (Qiagen, Hilden, Germany). Three biological replicates
257 of RNA from MM001i and MM008i tumors each were isolated using the Qiagen AllPrep DNA/RNA
258 Mini kit (Qiagen). Tumor tissues were mechanically homogenized in lysis buffer containing β-
259 mercaptoethanol using a glass Dounce homogenizer, followed by repeated aspiration through a
260 syringe for disruption. RNA quality was confirmed by Nanodrop spectrophotometer. Stranded
261 RNA-seq libraries were prepared in collaboration with the Genome Sequencing Facility at UT
262 Health for paired-end 100 bp sequencing. The sequencing raw reads were mapped to the mm10
263 *Mus Musculus* reference genome with HISAT2 v2.1.0[31], and gene counts were calculated with
264 htseq-count. Comprehensive gene expression data for cultured cells and tumors of each cell line
265 are available in Supplementary Table 1. Enrichment of KEGG signaling was conducted using the

266 top 1000 expressed genes of each cell line in each condition, with specific focus on immune
267 pathways, cancer cell pathways, and epithelial cell pathways. The input genes and enriched
268 pathways for MM001i and MM008i cultured cells and tumors are available in Supplementary Table
269 2. Differentially expressed genes in both datasets were identified with DEseq2 v1.40.2[32] by cutoff
270 of log2 fold change > 2 and adjusted *P* value < 0.01 for tumors and < 0.05 in culture (*P* value by
271 Wald test and *P* value adjustment by Benjamini-Hochberg adjustment).
272

273 **Single-cell expression profiling**

274 Three mammary tumors each of MM001i and MM008i were collected from six individual
275 mice. Single-cell suspensions were prepared for the 10X Genomics Chromium system using a
276 tumor dissociation kit (catalog no. 130-096-730, Miltenyi Biotec, San Diego, CA, USA) at a final
277 concentration of 1000 cells/uL. Single-cell RNA sequencing was performed in collaboration with
278 the Genome Sequencing Facility at UT Health according to the technical manual. Raw
279 sequencing reads were aligned to the mouse reference genome mm10 using 10x Genomics Cell
280 Ranger. Feature-barcode matrices were generated with Cell Ranger's count pipeline. Subsequent
281 analysis was performed in Seurat (v4.4.0)[33] using the following workflow: a Seurat object was
282 created with CreateSeuratObject using thresholds of min.cells = 3 (genes detected in ≥3 cells)
283 and min.features = 500 (cells expressing ≥500 genes). Cells with >30% mitochondrial transcript
284 content (percent.mt < 30) were excluded via subset. For MM001i, a total of 57,866 cells were
285 profiled and, after filtering, 40,645 cells remained in the analysis. For MM008i, 56,804 cells were
286 profiled and 39,726 cells remained after filtering. For each tumor model, cells were pooled and
287 clusters identified using FindClusters with a resolution parameter of 0.5. Cell types were identified
288 manually with curated cell markers: T cells: *Cd3g*, *Cd3d*, *Cd3e*, *Cd247*; B cells: *Cd19*, *B220*;
289 Macrophages: *Cd74*, *Cd14*, *Csf1r*; Endothelial cells: *Esam*, *Pecam1*; Stromal cells: *Fn1*, *Fap*,
290 *Acta2*, *S100a4*; Basal cells: *Krt14*, *Krt5*, *Krt17*; Epithelial cells: *Cdh1*, *Krt8*, *Krt18*, *Krt19*; Cancer
291 cells: *Acta2*, *Aldh1a3*, *Cd24a*, *Cdh1*, *Cdh2*, *Erbb2*, *Kit*, *Krt7*, *Mfge8*, *Myc*, *Pgr*, *Prlr*, *Tjp1*, *Top2a*,

292 *Twist1*.

293

294 **Nomenclature**

295 Throughout the manuscript, gene and transcript names are denoted with italics and protein
296 names with non-italics. All gene/protein names are capitalized fully regardless of species, except
297 for tumor gene expression analyses which use mouse nomenclature (first letter capitalized).

298

299 **Statistical analysis**

300 Calculations were done using Microsoft Excel software, and statistical analyses were
301 performed using GraphPad Prism software version 10.3.1 (GraphPad, La Jolla, CA, USA). Data
302 were plotted as means ± standard deviation. For tumor growth, Two-way analysis of variance
303 (ANOVA) was used to compare replicate means between multiple groups. Unpaired Student's *t*-
304 test was used to compare individual means. $P < 0.05$ was considered statistically significant.

305

306 **Results**

307 **Generation of murine mammary tumor cell lines MM001i and MM008i**

308 Two spontaneously arising mammary tumors were harvested from independent C57BL/6J
309 *MMTV-Cre p53*$^{fl/+}$ mice, and cell lines were generated by serial passage in culture and *in vivo*
310 (Supplementary Figure 1A; Materials and Methods). Primary tumors were isolated under sterile
311 conditions and expanded in culture to obtain sufficient cells for cryopreservation and engraftment
312 studies. 5 x 10^6 cells were injected into the mammary fat pad or subcutaneously in severely
313 immunocompromised NSG mice, and tumor formation occurred rapidly within 14-21 days as
314 expected in most animals regardless of injection site (not shown). However, parallel engraftments
315 of 5 x 10^6 cells into the same anatomical locations in fully immunocompetent C57BL/6J (WT)
316 animals only led to tumor formation in the mammary fat pad (Supplementary Figure 1).
317 Representative tumors from the first mammary fat pad engraftment were expanded in culture and

318 used in a second mammary fat pad engraftment. After two (MM001i) or three (MM008i) rounds of
319 culturing and engraftment, these cell lines formed stable and reproducible mammary tumors
320 (Supplementary Figure 1D,H). For post-tertiary mammary fat pad engraftments in WT mice, 2.5
321 $x10^6$ cells were sufficient to form tumors in 21-28 days with at least 70% efficiency. Therefore, this
322 cell number was used for all subsequent experiments.
323

324 **MM001i and MM008i tumors are potential models for human TNBC**

325 As these tumor cell lines had been generated from mice with mammary-specific
326 heterozygosity for *p53*, PCR was used to determine the genotype of this locus (Supplementary
327 Figure 2A; primers listed in methods).[28] Although both MM001i and MM008i harbored one *p53*
328 null allele (*i.e.*, *loxP*-to-*loxP* recombined) as anticipated, the WT allele could not be detected.
329 Taken together, these PCR results indicated that both MM001i and MM008i are functionally *p53*
330 homozygous null (likely through loss-of-heterozygosity early in tumor development).

331 Mammary tumor cell lines lacking functional p53 are typically also negative for the hormone
332 receptors, ER, PR, and HER2.[34, 35] To visualize these cell surface markers, representative tumors
333 from both MM001i and MM008i were formalin-fixed and paraffin-embedded for
334 immunohistochemical staining. MM001i and MM008i are both triple-negative at the protein level,
335 lacking positive nuclear staining of ER[36] and PR proteins[37] as well as cell surface staining of
336 HER2[38] (Supplementary Figure 2B).

337 Next, we used flow cytometry to quantify the surface expression of pro-tumorigenic,
338 immune co-signaling molecule PD-L1 on our cell lines at a basal levels and following 24 hrs
339 induction with interferon-gamma (IFN-γ)[12, 29]. MM008i showed higher expression of PD-L1 at basal
340 levels as well as after IFN-γ treatment compared to MM001i (Supplementary Figure 2C). However,
341 cell surface major histocompatibility complex-I (H-2KB) expression was similar between both cell
342 lines regardless of IFN-γ treatment (Supplementary Figure 2D).

343

344 **MM001i and MM008i respond differentially to αPD-1 but similarly to αCTLA-4**

345 After establishing a robust mammary fat pad engraftment protocol, WT females were split
346 randomly into subgroups and treated with the two most commonly used immunotherapy agents,
347 αPD-1 and αCTLA-4, to gauge therapy responsiveness. After engrafting on day 0 as above,
348 treatment with αPD-1, αCTLA-4, or the combination began on day 7, once tumors reached
349 approximately 200 mm^3. MM001i engrafted animals also received treatments on days 12 and 17
350 (Figure 1A). These tumors responded poorly to αPD-1 but regressed completely with αCTLA-4
351 monotherapy as well as with αPD-1 + αCTLA-4 combination therapy (Figure 1B). Non-
352 responsiveness was observed as expected in severely immunocompromised NSG mice (Figure
353 1C), indicating that these immunotherapy outcomes are immune response-dependent.

354 MM008i tumors were treated with a single dose on day 7 (Figure 1D). Additional doses
355 were not necessary because tumors regressed rapidly following this single treatment. MM008i
356 tumors responded equally well to both αPD-1 and αCTLA-4 monotherapies, ultimately leading in
357 most animals to complete tumor regression (Figure 1E). The combination of both mAbs appeared
358 to have no additional benefit (Figure 1E). The strong responsiveness to αPD-1 monotherapy
359 clearly distinguishes MM008i from MM001i. Moreover, neither tumor line appeared to be immune-
360 cold as evidenced by clear responses to αCTLA-4 monotherapy. As for MM001i tumors above,
361 no therapeutic benefit was observed for MM008i in NSG mice in any immunotherapy treatment
362 group, further consistent with an immune response-dependent mechanism of tumor regression
363 (Figure 1F).

364

365 **Immunotherapy of MM001i and MM008i tumors generates immune memory**

366 We next asked if immunotherapy treatment of MM001i and MM008i tumors triggers long-
367 lasting immune memory. Mice were engrafted with MM001i and MM008i and, beginning day 7,

368 treated as described above (workflows in Figure 2A,C). Mice demonstrating complete tumor
369 regression following αPD-1 and/or αCTLA-4 treatment were allowed to rest for 90 days and then
370 rechallenged through injection with the same tumor cell line at the same site as in the primary
371 injection. Age-matched female WT mice, which had never been injected with tumor cells
372 previously, were engrafted with MM001i and MM008i as controls. As expected, control mice with
373 *de novo* injections developed mammary tumors in 21-28 days following MM001i or MM008i
374 engraftment (Figure 2B,D). Conversely, all previously treated tumor-free mice rejected additional
375 engraftment attempts, thus indicating that both MM001i and MM008i are capable of provoking
376 long-term anti-tumor immune memory.
377

378 **$CD3^+$ T cells are distributed throughout MM008i unlike MM001i tumors**

379 Although MM001i and MM008i originated from the same genetic background, these two
380 mammary tumor cell lines exhibit starkly different responses to αPD-1 treatment (Figure 1). To
381 begin to investigate the underlying mechanism, immunohistochemistry was used to profile tumor-
382 infiltrating immune populations including as B and T lymphocytes. Untreated MM001i and MM008i
383 tumors were isolated after reaching the endpoint tumor volume of 1000 mm^3 and stained for CD19
384 and CD3 expression. Based on CD19 staining, B cell infiltration was low in both MM001i and
385 MM008i tumors (not shown). In contrast, both mammary tumors showed evidence for T cell
386 infiltration with MM008i tumors exhibiting significantly more $CD3^+$ T lymphocytes compared to
387 MM001i tumors (Figure 3A,B; positive control splenic $CD3^+$ cell staining in Supplementary Figure
388 3A). Moreover, T cells were localized throughout MM008i tumors versus predominantly around
389 the peripheral margins of MM001i tumors (Figure 3A). Deeper T lymphocyte penetration is
390 consistent with the possibility that this cell type may be responsible for the differential αPD-1
391 therapeutic outcomes of MM008i and MM001i tumors.
392

393 **Infiltrating CD8$^+$ T cells in MM008i tumors**

394 To further profile tumor-associated immune cells, flow cytometry was used to assess
395 specific immune cell subpopulations in treatment-naïve primary tumors. Following live cell gating,
396 a significantly higher percentage of CD45$^+$ immune cells was identified in MM008i tumors versus
397 MM001i tumors (Figure 3C; gating strategy and representative scatter plots in Supplementary
398 Figure 4). There was also a trend toward higher CD3$^+$ T cells out of CD45$^+$ immune cells (Figure
399 3D) and, interestingly, a significantly higher percentage of CD8$^+$CD4$^-$ cytotoxic T cells in the CD3$^+$
400 population of MM008i tumors (Figure 3E). Additionally, activated, pre-exhausted PD-1$^+$TIM3$^-$CD8$^+$
401 T cells[12, 39] were significantly higher, though no difference was observed for exhausted PD-
402 1$^+$TIM3$^+$ T cells in MM008i compared to MM001i tumors (Figure 3F,G).[40, 41] No significant
403 difference was observed for CD11b$^+$ monocytes, CD11b$^+$Gr1$^+$ myeloid-derived suppressor cells,
404 or B220$^+$ B cells (Supplementary Figure 3B,C,D). A trend towards a higher percentage of
405 CD11b$^+$CD11c$^+$ dendritic cells and NK1.1$^+$ natural killer cells was observed in MM001i tumors,
406 though it was not statistically significant (Supplementary Figure 3E,F). These observations
407 combine to indicate that the successful αPD-1 outcomes observed for MM008i tumor-engrafted
408 animals may be mediated through pre-exhausted PD-1$^+$TIM3$^-$CD8$^+$ T cells.

409

410 **Depletion of CD8$^+$ cells abrogates αPD-1 treatment efficacy in MM008i**

411 The aforedescribed results suggest that the αPD-1 responsiveness of MM008i may be
412 due to infiltrating anti-tumor CD8$^+$ T cells. To test this possibility directly, experiments were
413 performed in which CD8$^+$ T cells were immunodepleted from animals before and after MM008i
414 tumor treatment with αPD-1 (workflow in Figure 4A). Tumors showed normal growth kinetics in
415 WT animals treated with isotype control mAbs or an αCD8 mAb (Figure 4B). As above, αPD-1
416 treatment alone resulted in near-complete tumor regression (Figure 4B). However, three doses of
417 αCD8 mAb (one before and two after αPD-1 treatment) were sufficient to blunt the therapeutic

418 responsiveness of the αPD-1 therapy (Figure 4B). Immunohistochemistry confirmed depletion of
419 $CD8^+$ T lymphocytes from MM008i tumors (representative images in Figure 4C). These data
420 combined to show that $CD8^+$ T cells are an integral cell population required for MM008i tumor
421 regression in response to αPD-1 therapy in WT mice.
422
423 **RNA-sequencing of MM001i and MM008i cells**
424 To identify tumor-intrinsic factors that contribute to the differential responsiveness to αPD-
425 1, bulk RNA sequencing was done for cultured asynchronous MM001i and MM008i cell
426 populations (2 independent cultures per line) and for untreated tumors from animals (3
427 independent tumors per line). A full list of expressed genes from cultured cells and untreated
428 tumors is provided in Supplementary Table 1. First, as expected from initial genotyping above, no
429 transcripts were detected for *p53* exons 2-10 confirming *p53* loss of function. Second, multiple
430 breast cancer-associated genes were expressed at similar levels in both cell lines (*Brca1, Brca2,*
431 *Mki67, Myc, Pik3ca*, *Pten*, *Rb1*) with no apparent disease mutations. Third, consistent with IHC
432 results above, *Esr1* transcripts were not detected in either cell line. Fourth, in contrast to the IHC
433 results above where HER2 was not detected, both lines appear to express similar levels of *Erbb2*
434 RNA. This inconsistency may be due to an intrinsic cellular defect prior to translation as this
435 protein was undetectable by IHC and unlikely to be retained intracellularly. Finally, modest levels
436 of *Ar* and *Pgr* RNA were observed in MM001i cultured cells, and not in MM008i. Expression
437 comparisons were less clear in bulk RNA from tumors due to a multitude of normal infiltrating cell
438 types.
439 To evaluate broad expression differences between MM001i and MM008i cells and tumors,
440 we used principal component analysis (PCA) to compare the overall transcription profiles for
441 MM001i and MM008i in each growth condition (Supplementary Figure 5A). In general, cultured
442 cells clustered closely together as anticipated. In comparison, tumor cells clustered far away from

443 cultured cells and in more loosely associated groups consistent with differential immune
444 responses. We next analyzed specific gene expression differences between MM001i and
445 MM008i, identified based on a greater than 4-fold change and *P* values < 0.05 for cultured cells
446 and < 0.01 for untreated tumors (Figure 5A; Supplementary Table 1). Among the highest
447 differentially expressed genes are immune related genes, such as *Il11*, *Cxcl2*, *Il7*, *Il1rap*, *Ifnlr1*,
448 and *Cxcl3* in tumors, *Tnf* and *Havcr2* (encoding TIM3) in cultured cells, and *Il1rl1*, *Nfgr*, and *Ptgs2*
449 in both sets, which could potentially relate to the observed differences in response to αPD-1
450 therapy and in T lymphocyte infiltration.

451 To evaluate gene expression at the pathway level, we conducted KEGG signaling pathway
452 analysis on the top 1000 expressed genes in MM001i and MM008i cells and tumors, focusing
453 specifically on enriched pathways in immune signaling, cancer, and epithelial cell development
454 (Supplementary Figure 5B; Supplementary Table 2). Overall, gene expression was very similar
455 between MM001i and MM008i, particularly in epithelial cell signaling pathways. MM008i tumors
456 were relatively enriched for immune related pathways such as antigen processing and
457 presentation, and phagosome, with genes such as *H2-t23* and *B2m* being among the most
458 strongly expressed. Conversely, MM001i tumors were relatively enriched for cancer related
459 pathways such as extracellular matrix (ECM)-receptor interaction and PI3K-AKT signaling. These
460 gene expression insights highlight the many similarities between MM001i and MM008i mammary
461 tumor cell models and also point toward differences that may explain the differential
462 responsiveness to immune therapy.

463

464 **Single-cell profiling of MM001i and MM008i tumors**

465 Single cell (sc)RNA-seq analysis of untreated MM001i and MM008i tumors freshly isolated
466 from mice revealed additional intrinsic and extrinsic features of each tumor cell line. Unsupervised
467 clustering (UMAP) identified major cell types, including normal and cancer epithelial cells,
468 endothelial cells, stromal cells, basal cells, and immune populations (Figure 5B,C). Epithelial cells

469 in both MM001i and MM008i exhibited elevated expression of the oncogenes *Myc* and *Top2a*,
470 indicating shared proliferative and malignant transcriptional programs (Figure 5D). *Ctla-4* (*CTLA-*
471 *4*) and *Pdcd1* (*PD-1*) were highly expressed in T cells of both MM001i and MM008i, whereas the
472 mRNA for the CTLA-4 ligand *Cd86* showed no significant upregulation in either MM001i or
473 MM008i (Figure 5D). In contrast, *Cd274* (encoding PD-L1) was overexpressed specifically in
474 epithelial cells of MM008i but not in epithelial cells of MM001i, implying specific immune evasion
475 via the PD-1/PD-L1 axis in MM008i tumors (Figure 5D).
476

477 **Discussion**

478 We report the development of two syngeneic murine mammary tumor cell lines that,
479 despite originating from the same C57BL/6J genetic background, display differential *in vivo*
480 responsiveness to αPD-1 checkpoint blockade. Specifically, the mammary tumor cell line MM008i
481 tumors responds to αPD-1 therapy and MM001i does not. However, both lines are fully responsive
482 to αCTLA-4 therapy, and tumor clearance associates with immunity to subsequent engraftment.
483 Moreover, comparative immune cell profiling of engrafted tumors showed higher percentages of
484 $CD8^+$ cytotoxic T cells in MM008i tumors compared to MM001i tumors. These $CD8^+$ T lymphocytes
485 are required for response to αPD-1 in MM008i tumors, as depletion of this population abrogates
486 therapy response. Another key difference we identified was significantly higher expression of PD-
487 L1 on MM008i epithelial cells compared to MM001i. This strongly indicates that the PD-1/PD-L1
488 axis is a major mediator of immune evasion in MM008i, which is reflective of αPD-1 clinical
489 observations in breast cancer where PD-L1 serves as a key biomarker for positive responses.[11,
490 42, 43] However, despite these clear phenotypic differences between tumors, MM001i and MM008i
491 are overall very similar at the gene expression level. We observed similar expression levels of
492 commonly dysregulated breast cancer genes such as *Brca1, Brca2, Mki67, Myc, Pik3ca*, *Pten*,
493 *Rb1*, and *Top2a*, and similarities in epithelial signaling pathways.

494 The mammary tumor models presented help fill an important gap in syngeneic systems
495 for preclinical immune therapy testing and mechanistic studies. Syngeneic mammary tumor
496 models are rare, with only a few described to date.[14, 18, 21, 24-26, 44] E0771, which has been around
497 for 70 years and with unknown passage number, has conflicting reports on ER hormone receptor
498 status.[18] Other lines, such as PyMT,[24] AT-3,[25] and WT145[26] rely on either transgene insertion or
499 chemical carcinogens to drive cancer formation, processes that do not reflect cancer development
500 in human patients. Further, it would be difficult to compare results across lines given substantial
501 differences between each in genetic background, growth kinetics, and immune phenotype, limiting
502 the potential for comparative analysis. To address some of these limitations, recent efforts have
503 focused on developing new models that better recapitulate the immunological characteristics of
504 human disease.[45] However, many of these models are poorly responsive to immunotherapy,
505 owing to low tumor mutational burdens, unless further modified by induced mutagenesis or *Brca1*
506 deficiency.[45] Our new models, which exhibit clear responses to αCTLA-4 and differential
507 responses to αPD-1, provide a unique platform to dissect mechanisms of immunotherapy
508 resistance and test additional therapies (alone and in combination).

509 In particular, we envision our mammary tumor models being used to test other therapies
510 in combination with αPD-1 for potential dosage de-escalation of MM008i and to potentially trigger
511 αPD-1 responsiveness to MM001i. Our TNBC models also may be used to dissect the tumor
512 microenvironment itself, particularly focusing on extracellular matrix signaling and immune
513 infiltration. Here, we demonstrate considerable differences in T cell infiltration between our
514 MM001i and MM008i tumors. However, we have not directly investigated the specific mechanisms
515 which permit greater immune infiltration in MM008i tumors than MM001i tumors. We anticipate
516 future studies looking more deeply into these two cell lines immunologically, particularly the factors
517 that influence whether a tumor is “immune hot” or “immune cold”. By identifying some of these
518 molecular determinants, we may be able to identify combination therapy approaches to make

519 previously resistant tumors sensitive to immunotherapies.

520

521 **Acknowledgments**

522 We thank Francesca Manara (Memorial Sloan Kettering Cancer Center), Josephine
523 Taverna (UT Health San Antonio), and Ratna Vadlamudi (UT Health San Antonio) for thoughtful
524 feedback, and Emily Law, Jordan Naumann, and Angel Dominguez for early contributions to this
525 project. We are also grateful to Zhao Lai at the UT Health San Antonio Genome Sequencing
526 Facility for assistance with library preparation and sequencing and to the South Texas Research
527 Histology Laboratory for help with mouse specimen processing.

528

529 **Disclosure statement**

530 No potential conflict of interest was reported by the authors.

531

532 **Funding**

533 These studies were supported by NCI P50-CA247749, NCI P01-CA234228, and a
534 Recruitment of Established Investigators Award from the Cancer Prevention and Research
535 Institute of Texas (CPRIT RR220053). T.J.K. was supported in part by the STX-MSTP NIH training
536 grants (T32GM113896 and T32GM145432), as well as the Translational Science Training T32
537 Award (T32TR004545). C.D. was supported in part by a CPRIT Research Training Award (RP
538 170345). I.T. was also supported in part by NIH T32GM145432. R.S.H. is an Investigator of the
539 Howard Hughes Medical Institute, a CPRIT Scholar, and the Ewing Halsell President's Council
540 Distinguished Chair at the UT Health San Antonio. The UT Health San Antonio Genome
541 Sequencing Facility is supported by NCI P30-CA054174 (Mays Cancer Center at UT Health San
542 Antonio) and NIH Shared Instrument grant S10-OD030311 (S10 grant to NovaSeq 6000 System),
543 and CPRIT Core Facility Award (RP220662). The funders had no roles in study design, data
544 collection and analysis, decision to publish, or preparation of the manuscript.

Author contributions

Reuben S. Harris, Harshita B. Gupta: Conceptualized the project; Thomas J. Kalantzakos, Harshita B. Gupta, Cameron Durfee, Anusha Soni, Benjamin Troness: Conducted *in vivo* experimentation; Xingyu Liu, Joshua Proehl, Harshita B. Gupta, Ian Tamayo: Performed immunohistochemistry; Yufan Zhou, Xingyu Liu, Nuri Alpay Temiz: Contributed to computational analyses; Thomas J. Kalantzakos, Harshita B. Gupta: Performed cell-based experiments; Thomas J. Kalantzakos, Harshita B. Gupta, Reuben S. Harris: Drafted the manuscript with all authors contributing to manuscript proofing and revision.

Data availability statement

The murine mammary tumor cell lines generated in this study, MM001i and MM008i, are available through the American Type Culture Collection or written request. Primary bulk and single-cell RNAseq data sets are available through GEO (GSE305800 and GSE305842; respectively https://www.ncbi.nlm.nih.gov/geo/query/acc.cgi?acc=GSE305800 and https://www.ncbi.nlm.nih.gov/geo/query/acc.cgi?acc=GSE305842. Supplementary Tables 1 and 2 are available on Figshare (doi: 10.6084/m9.figshare.30468098) using the link https://figshare.com/s/cd92140dd5a6f2f5a9d4. All other primary data are presented in the manuscript. A preprint of this work is also available on *bioRxiv* (https://www.biorxiv.org/content/10.1101/2025.09.18.677171v1).

References

1. Menon G, Alkabban FM, Ferguson T. Breast cancer. *StatPearls* Treasure Island (FL)2024.
2. Nolan E, Lindeman GJ, Visvader JE. Deciphering breast cancer: from biology to the clinic. *Cell* 2023;186(8):1708-28.

570 3. Almansour NM. Triple-negative breast cancer: a brief review about epidemiology, risk factors,
571 signaling pathways, treatment and role of artificial intelligence. *Front Mol Biosci*
572 2022;9:836417.
573 4. Dent R, Trudeau M, Pritchard KI, Hanna WM, Kahn HK, Sawka CA, et al. Triple-negative breast
574 cancer: clinical features and patterns of recurrence. *Clin Cancer Res* 2007;13(15 Pt
575 1):4429-34.
576 5. Liedtke C, Mazouni C, Hess KR, Andre F, Tordai A, Mejia JA, et al. Response to neoadjuvant
577 therapy and long-term survival in patients with triple-negative breast cancer. *J Clin Oncol*
578 2008;26(8):1275-81.
579 6. Darb-Esfahani S, Denkert C, Stenzinger A, Salat C, Sinn B, Schem C, et al. Role of TP53
580 mutations in triple negative and HER2-positive breast cancer treated with neoadjuvant
581 anthracycline/taxane-based chemotherapy. *Oncotarget* 2016;7(42):67686-98.
582 7. Cancer Genome Atlas N. Comprehensive molecular portraits of human breast tumours. *Nature*
583 2012;490(7418):61-70.
584 8. Bakhtiar H, Sharifi MN, Helzer KT, Shi Y, Bootsma ML, Shang TA, et al. A phenocopy signature
585 of TP53 loss predicts response to chemotherapy. *NPJ Precis Oncol* 2024;8(1):220.
586 9. Lehmann BD, Bauer JA, Chen X, Sanders ME, Chakravarthy AB, Shyr Y, et al. Identification of
587 human triple-negative breast cancer subtypes and preclinical models for selection of
588 targeted therapies. *J Clin Invest* 2011;121(7):2750-67.
589 10. Schmid P, Cortes J, Pusztai L, McArthur H, Kummel S, Bergh J, et al. Pembrolizumab for early
590 triple-negative breast cancer. *N Engl J Med* 2020;382(9):810-21.
591 11. Cortes J, Rugo HS, Cescon DW, Im SA, Yusof MM, Gallardo C, et al. Pembrolizumab plus
592 chemotherapy in advanced triple-negative breast cancer. *N Engl J Med* 2022;387(3):217-
593 26.

594 12. Nederlof I, Isaeva OI, de Graaf M, Gielen R, Bakker NAM, Rolfes AL, et al. Neoadjuvant
595 nivolumab or nivolumab plus ipilimumab in early-stage triple-negative breast cancer: a
596 phase 2 adaptive trial. *Nat Med* 2024;30(11):3223-35.
597 13. Li Q, Liu J, Zhang Q, Ouyang Q, Zhang Y, Liu Q, et al. The anti-PD-L1/CTLA-4 bispecific
598 antibody KN046 in combination with nab-paclitaxel in first-line treatment of metastatic
599 triple-negative breast cancer: a multicenter phase II trial. *Nat Commun* 2024;15(1):1015.
600 14. Goodson LH, Barvick L, Stone RG, Ibach M, Palmer J. Inhibition screening data using
601 sarcoma 180 and adenocarcinoma E0771. *Cancer Res* 1955;Suppl. 2:81-102.
602 15. Kasikara C, Davra V, Calianese D, Geng K, Spires TE, Quigley M, et al. Pan-TAM Tyrosine
603 Kinase Inhibitor BMS-777607 Enhances anti-PD-1 mAb efficacy in a murine model of
604 triple-negative breast cancer. *Cancer Res* 2019;79(10):2669-83.
605 16. Liu J, Blake SJ, Yong MC, Harjunpaa H, Ngiow SF, Takeda K, et al. Improved efficacy of
606 neoadjuvant compared to adjuvant immunotherapy to eradicate metastatic disease.
607 *Cancer Discov* 2016;6(12):1382-99.
608 17. Zheng X, Fang Z, Liu X, Deng S, Zhou P, Wang X, et al. Increased vessel perfusion predicts
609 the efficacy of immune checkpoint blockade. *J Clin Invest* 2018;128(5):2104-15.
610 18. Le Naour A, Rossary A, Vasson MP. EO771, is it a well-characterized cell line for mouse
611 mammary cancer model? Limit and uncertainty. *Cancer Med* 2020;9(21):8074-85.
612 19. Johnstone CN, Smith YE, Cao Y, Burrows AD, Cross RS, Ling X, et al. Functional and
613 molecular characterisation of EO771.LMB tumours, a new C57BL/6-mouse-derived model
614 of spontaneously metastatic mammary cancer. *Dis Model Mech* 2015;8(3):237-51.
615 20. Gu JW, Young E, Busby B, Covington J, Johnson JW. Oral administration of pyrrolidine
616 dithiocarbamate (PDTC) inhibits VEGF expression, tumor angiogenesis, and growth of
617 breast cancer in female mice. *Cancer Biol Ther* 2009;8(6):514-21.

618 21. Aslakson CJ, Miller FR. Selective events in the metastatic process defined by analysis of the
619 sequential dissemination of subpopulations of a mouse mammary tumor. *Cancer Res*
620 1992;52(6):1399-405.
621 22. Kim K, Skora AD, Li Z, Liu Q, Tam AJ, Blosser RL, et al. Eradication of metastatic mouse
622 cancers resistant to immune checkpoint blockade by suppression of myeloid-derived cells.
623 *Proc Natl Acad Sci U S A* 2014;111(32):11774-9.
624 23. Taylor MA, Hughes AM, Walton J, Coenen-Stass AML, Magiera L, Mooney L, et al.
625 Longitudinal immune characterization of syngeneic tumor models to enable model
626 selection for immune oncology drug discovery. *J Immunother Cancer* 2019;7(1):328.
627 24. Yan C, Yang J, Saleh N, Chen SC, Ayers GD, Abramson VG, et al. Inhibition of the PI3K/mTOR
628 pathway in breast cancer to enhance response to immune checkpoint inhibitors in breast
629 cancer. *Int J Mol Sci* 2021;22(10).
630 25. Stewart TJ, Abrams SI. Altered immune function during long-term host-tumor interactions can
631 be modulated to retard autochthonous neoplastic growth. *J Immunol* 2007;179(5):2851-9.
632 26. Zinser GM, McEleney K, Welsh J. Characterization of mammary tumor cell lines from wild
633 type and vitamin D3 receptor knockout mice. *Mol Cell Endocrinol* 2003;200(1-2):67-80.
634 27. Percie du Sert N, Hurst V, Ahluwalia A, Alam S, Avey MT, Baker M, et al. The ARRIVE
635 guidelines 2.0: updated guidelines for reporting animal research. *BMJ Open Sci*
636 2020;4(1):e100115.
637 28. Marino S, Vooijs M, van Der Gulden H, Jonkers J, Berns A. Induction of medulloblastomas in
638 p53-null mutant mice by somatic inactivation of Rb in the external granular layer cells of
639 the cerebellum. *Genes Dev* 2000;14(8):994-1004.
640 29. Gupta HB, Clark CA, Yuan B, Sareddy G, Pandeswara S, Padron AS, et al. Tumor cell-intrinsic
641 PD-L1 promotes tumor-initiating cell generation and functions in melanoma and ovarian
642 cancer. *Signal Transduct Target Ther* 2016;1:16030-.

643 30. Durfee C, Temiz NA, Levin-Klein R, Argyris PP, Alsoe L, Carracedo S, et al. Human
644 APOBEC3B promotes tumor development in vivo including signature mutations and
645 metastases. *Cell Rep Med* 2023;4(10):101211.
646 31. Kim D, Paggi JM, Park C, Bennett C, Salzberg SL. Graph-based genome alignment and
647 genotyping with HISAT2 and HISAT-genotype. *Nat Biotechnol* 2019;37(8):907-15.
648 32. Love MI, Huber W, Anders S. Moderated estimation of fold change and dispersion for RNA-
649 seq data with DESeq2. *Genome Biol* 2014;15(12):550.
650 33. Hao Y, Hao S, Andersen-Nissen E, Mauck WM, 3rd, Zheng S, Butler A, et al. Integrated
651 analysis of multimodal single-cell data. *Cell* 2021;184(13):3573-87 e29.
652 34. Knight JF, Lesurf R, Zhao H, Pinnaduwage D, Davis RR, Saleh SM, et al. Met synergizes with
653 p53 loss to induce mammary tumors that possess features of claudin-low breast cancer.
654 *Proc Natl Acad Sci U S A* 2013;110(14):E1301-10.
655 35. Wang S, Liu JC, Kim D, Datti A, Zacksenhaus E. Targeted Pten deletion plus p53-R270H
656 mutation in mouse mammary epithelium induces aggressive claudin-low and basal-like
657 breast cancer. *Breast Cancer Res* 2016;18(1):9.
658 36. Bruner-Tran KL, Duleba AJ, Taylor HS, Osteen KG. Developmental toxicant exposure is
659 associated with transgenerational adenomyosis in a murine model. *Biol Reprod*
660 2016;95(4):73.
661 37. Zhao W, Wang Y, Liu J, Yang Q, Zhang S, Hu X, et al. Progesterone activates the histone
662 lactylation-Hif1alpha-glycolysis feedback loop to promote decidualization. *Endocrinology*
663 2023;165(1).
664 38. Choudhury S, Ghosh S, Chakraborty P, Pal S, Ghosh K, Saha S, et al. Epidermal growth
665 factor receptor (EGFR) and SMAD4 negatively correlated in the progression of gallbladder
666 cancer in Eastern Indian patients. BMC Gastroenterol 2024;24(1):446.

667 39. Kinget L, Naulaerts S, Govaerts J, Vanmeerbeek I, Sprooten J, Laureano RS, et al. A spatial
668 architecture-embedding HLA signature to predict clinical response to immunotherapy in
669 renal cell carcinoma. *Nat Med* 2024;30(6):1667-79.
670 40. Jin HT, Anderson AC, Tan WG, West EE, Ha SJ, Araki K, et al. Cooperation of Tim-3 and PD-
671 1 in CD8 T-cell exhaustion during chronic viral infection. *Proc Natl Acad Sci U S A*
672 2010;107(33):14733-8.
673 41. Sakuishi K, Apetoh L, Sullivan JM, Blazar BR, Kuchroo VK, Anderson AC. Targeting Tim-3
674 and PD-1 pathways to reverse T cell exhaustion and restore anti-tumor immunity. *J Exp*
675 *Med* 2010;207(10):2187-94.
676 42. James JL, Balko JM. Biomarker predictors for immunotherapy benefit in breast: beyond PD-
677 L1. *Curr Breast Cancer Rep* 2019;11(4):217-27.
678 43. Khan M, Du K, Ai M, Wang B, Lin J, Ren A, et al. PD-L1 expression as biomarker of efficacy
679 of PD-1/PD-L1 checkpoint inhibitors in metastatic triple negative breast cancer: A
680 systematic review and meta-analysis. *Front Immunol* 2023;14:1060308.
681 44. Perez-Lanzon M, Carbonnier V, Cordier P, De Palma FDE, Petrazzuolo A, Klein C, et al. New
682 hormone receptor-positive breast cancer mouse cell line mimicking the immune
683 microenvironment of anti-PD-1 resistant mammary carcinoma. *J Immunother Cancer*
684 2023;11(6).
685 45. Hollern DP, Xu N, Thennavan A, Glodowski C, Garcia-Recio S, Mott KR, et al. B cells and T
686 follicular helper cells mediate response to checkpoint inhibitors in high mutation burden
687 mouse models of breast cancer. *Cell* 2019;179(5):1191-206 e21.
688
689

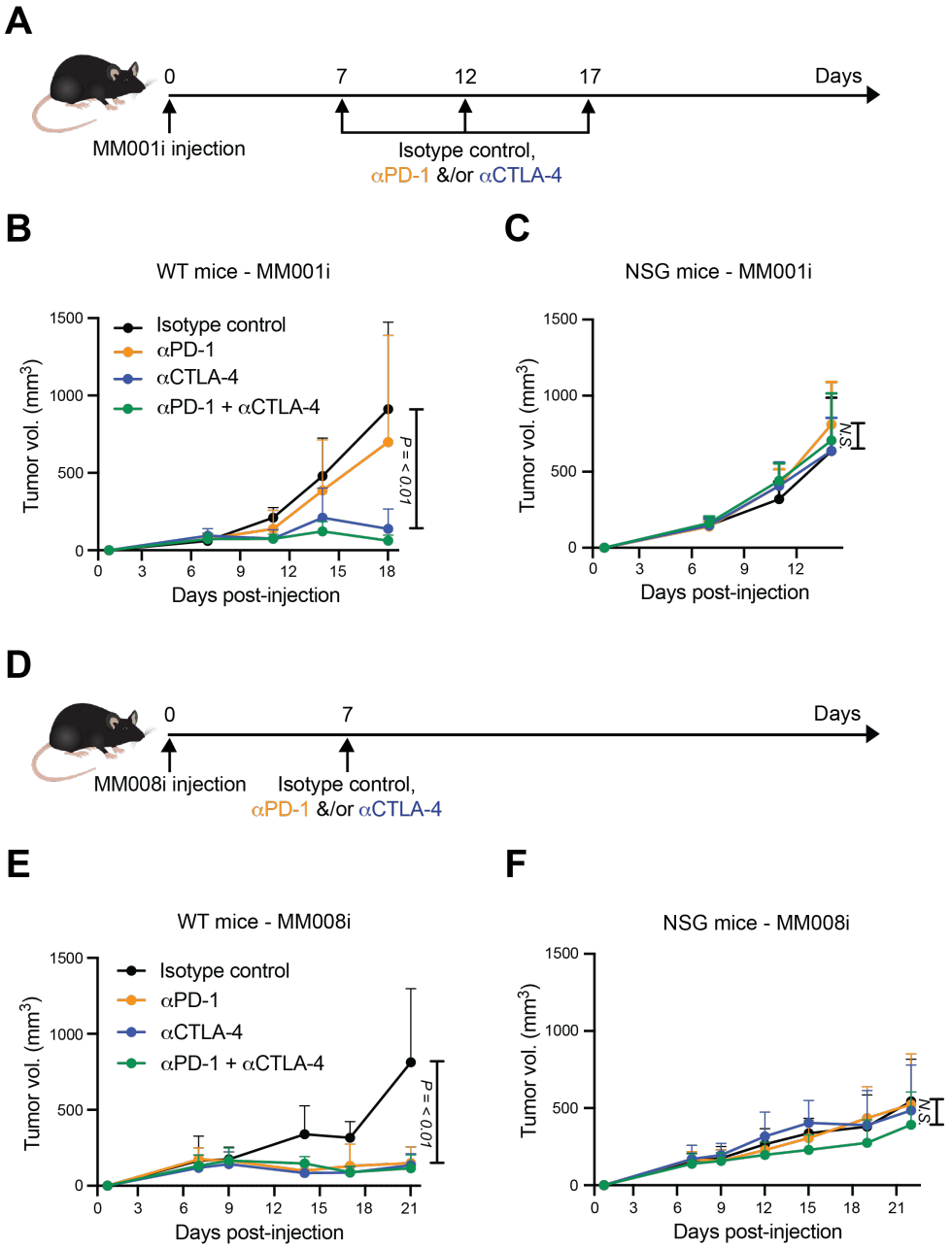

Figure 1. MM001i and MM008i tumors exhibit differential immunotherapy responsiveness.

(**A**) Timeline of MM001i tumor injection and treatment with αPD-1 ± αCTLA-4 or isotype controls. (**B-C**) Tumor growth curves of MM001i following injection into the mammary fat pads of WT or severely immunocompromised (NSG) female mice, respectively, in the indicated treatment groups. n=6 (WT) or 4 (NSG) animals per group with two tumors per mouse; *P*-values using two-way ANOVA.

(**D**) Timeline of MM008i tumor injection and treatment with αPD-1 ± αCTLA-4 or isotype controls. (**E-F**) Tumor growth curves of MM001i following injection into the mammary fat pads of WT or NSG female mice, respectively, in the indicated treatment groups. n=6 (WT) or 4 (NSG) animals per group with two tumors per mouse; *P*-values using two-way ANOVA.

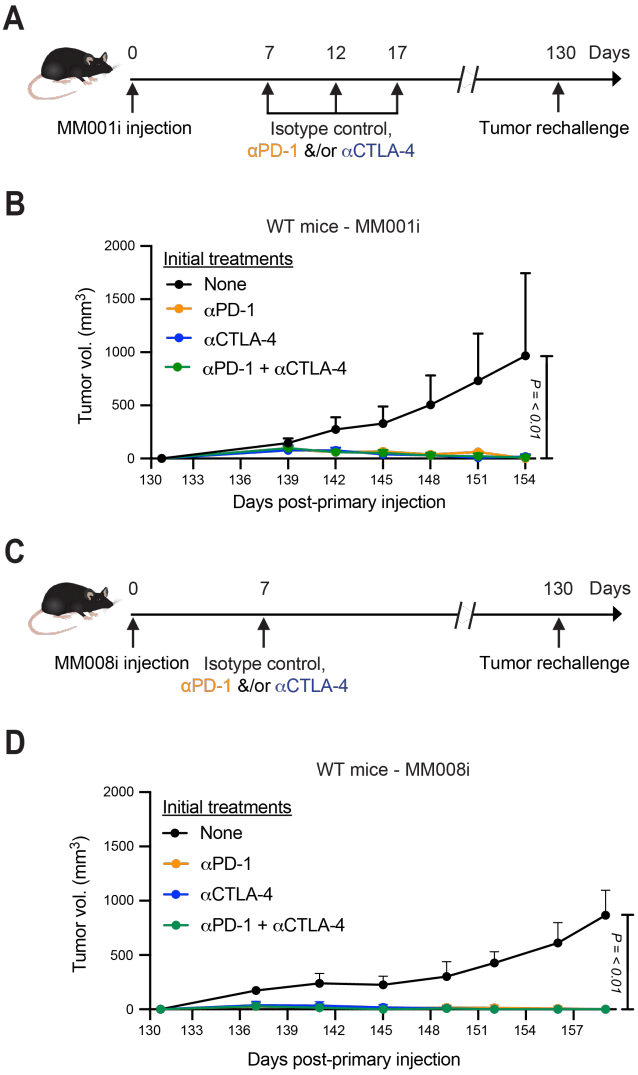

Figure 2. MM001i and MM008i tumors elicit durable immune memory response post-immunotherapy treatments.

(**A**) Timeline of initial and subsequent MM001i tumor injections and treatment with αPD-1, αCTLA-4, or combination.

(**B**) Tumor growth curves of MM001i following second tumor engraftment into WT female mice. n=4 animals per group (1 mouse for αPD-1) with two tumors per mouse; *P*-values using two-way ANOVA.

(**C**) Timeline of initial and subsequent MM008i tumor injections and treatment with αPD-1, αCTLA-4, or combination.

(**D**) Tumor growth curves of MM008i following second tumor engraftment into WT female mice. n=5 animals per group with two tumors per mouse; *P*-values using two-way ANOVA.

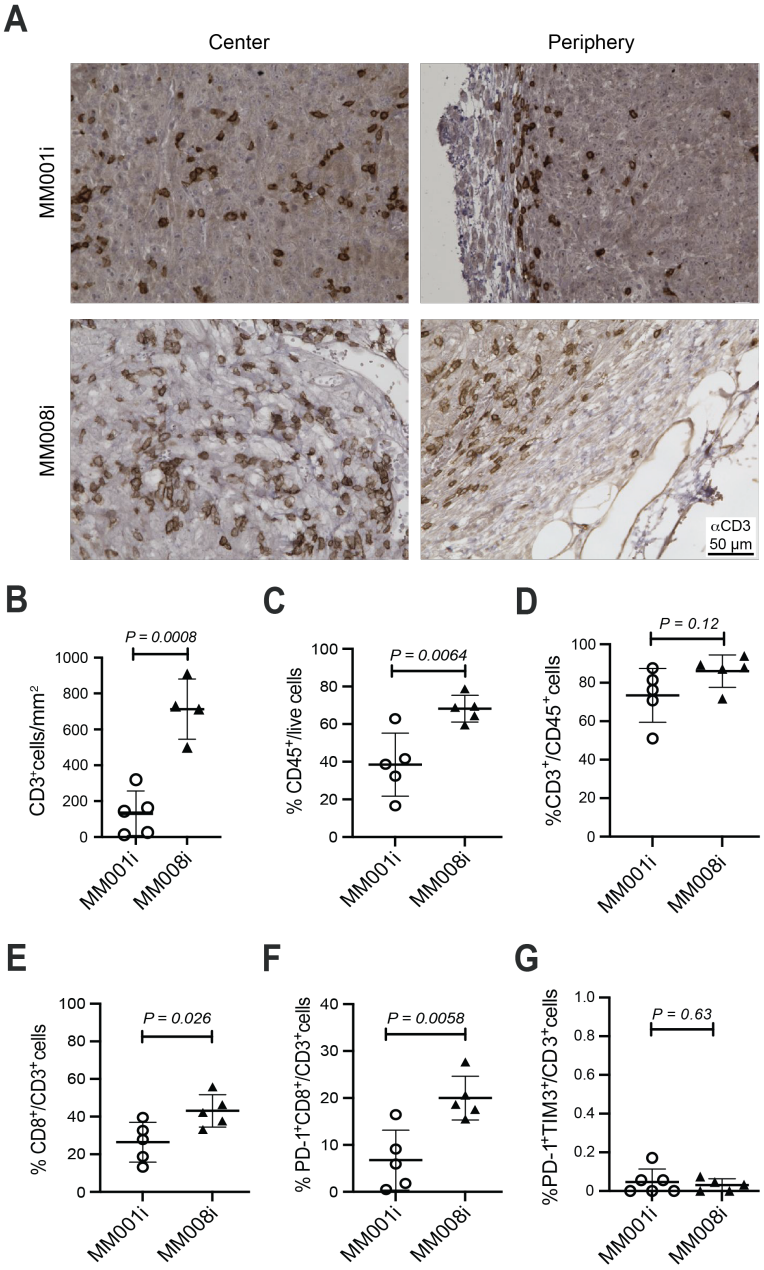

Figure 3. MM008i tumors are enriched with total T cells and pre-exhausted PD-1$^+$CD8$^+$ T cells compared to MM001i tumors.

(**A**) Representative αCD3 IHC images of untreated MM001i and MM008i tumors.

(**B**) Quantification of CD3$^+$ T cells/mm^3 in untreated MM001i and MM008i tumors using QuPath bioimage analysis software (5 random uniform regions of interest per tumor; n=5 tumors for MM001i, and 4 tumors for MM008i; *P*-value by unpaired Student's *t*-test).

(**C-G**) Immune cell infiltrates with the indicated cell surface markers as estimated by flow cytometry (n=4-5 tumors per group; *P*-value by unpaired Student's *t*-test).

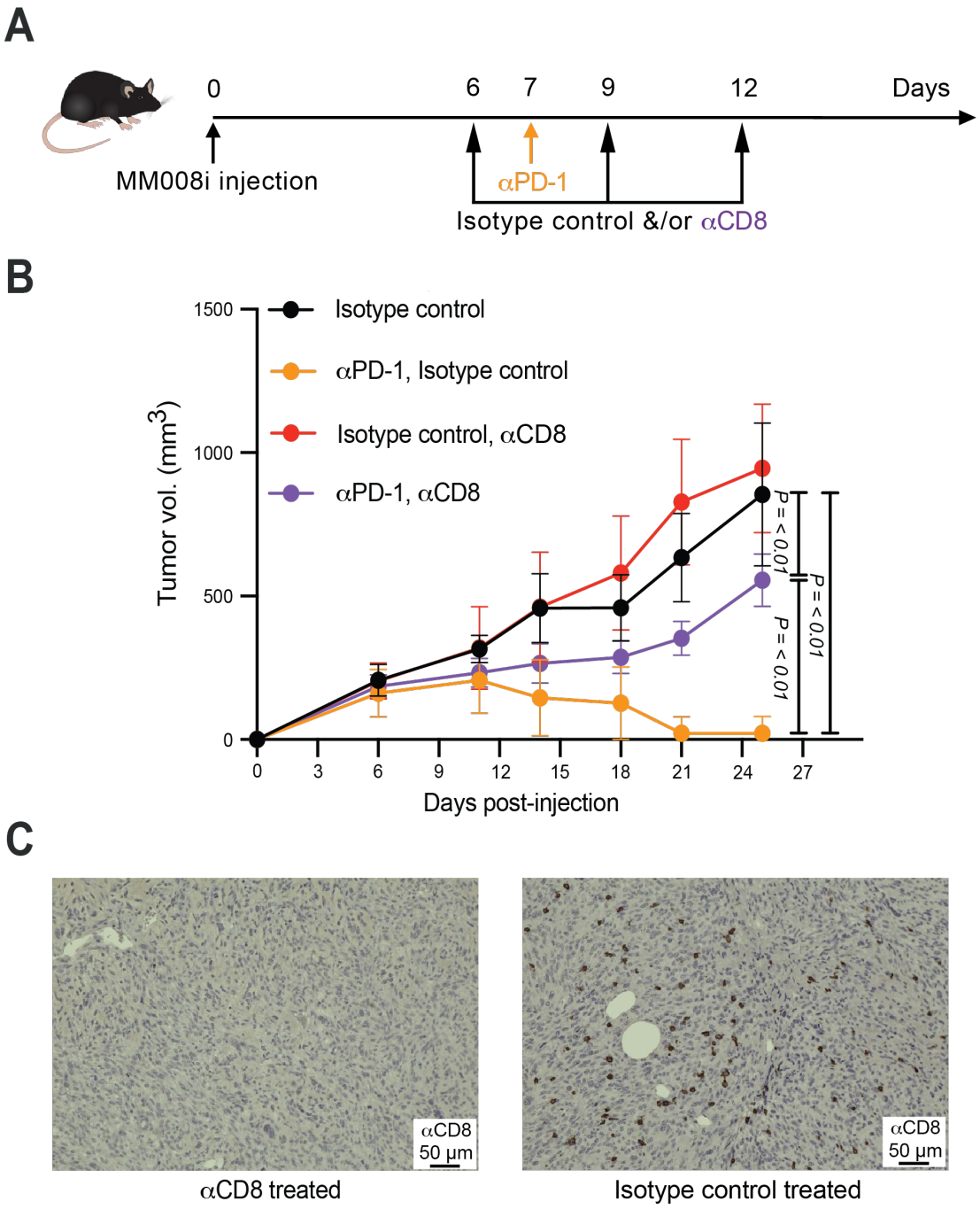

Figure 4. αCD8 neutralizing antibody abrogates αPD-1 response in MM008i tumors.

(**A**) Timeline of MM008i tumor injections and treatments with αPD-1 ± αCD8 or isotype controls.

(**B**) Tumor growth curves of MM008i following tumor injection in WT females in the indicated treatment groups. n=5 animals per group with two tumors/mouse; *P*-values using two-way ANOVA.

(**C**) Reconstruction experiment showing representative αCD8 IHC images of MM008i tumors on day 13, immediately following treatment of animals with αCD8 neutralizing antibody or an isotype control antibody.

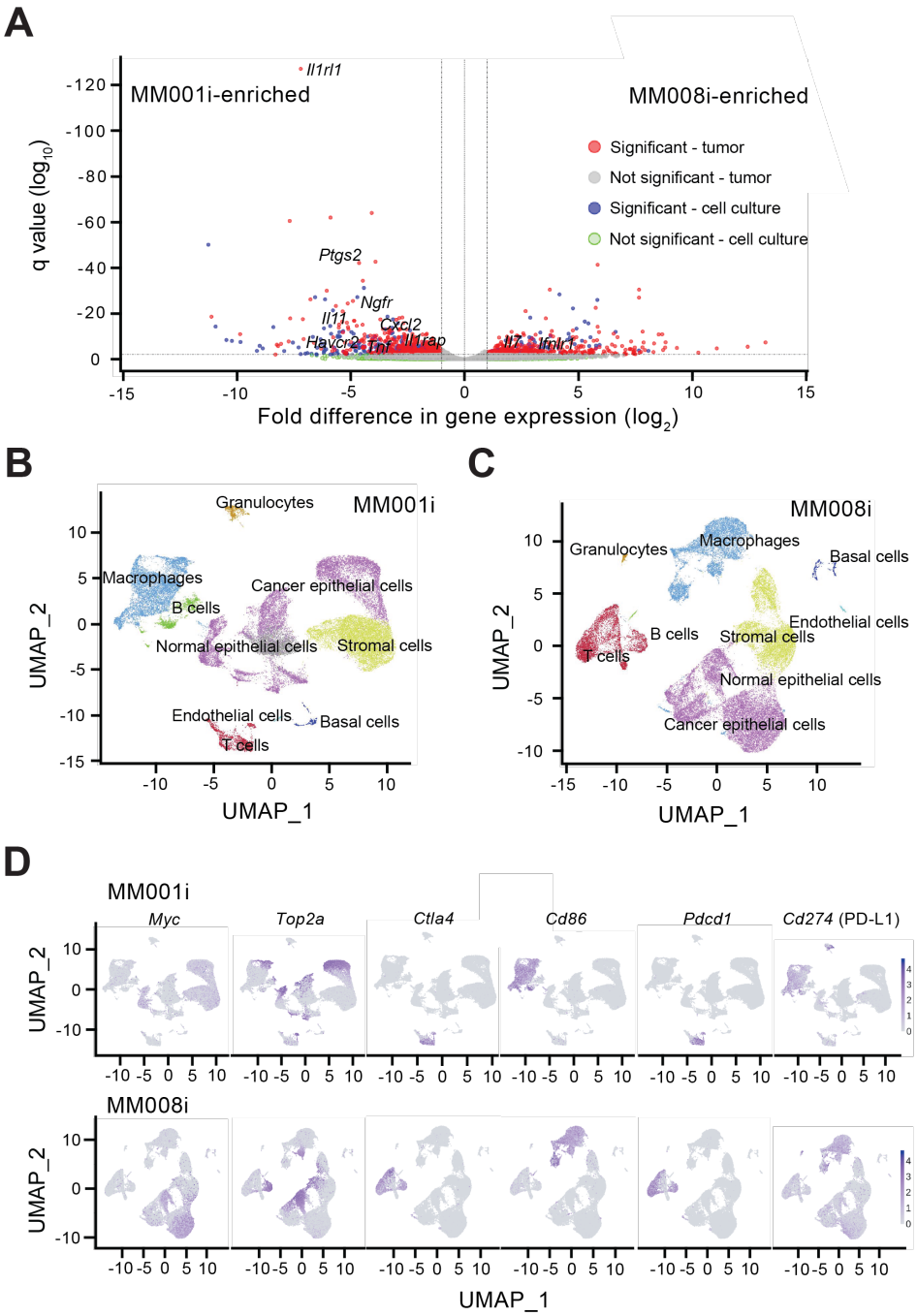

Figure 5. Gene expression profiling of MM001i and MM008i tumors.

(**A**) Volcano plot depicting differentially expressed genes between MM001i and MM008i cells in culture and tumors *in vivo* by RNA-seq (filtered by $\log_2$-fold change > 2 and adjusted *P*-value <0.05 for cultured cells and < 0.01 for tumors)**.**

(**B-C**) UMAP clustering of MM001i and MM008i tumors, respectively, with cell type annotations by single-cell RNA-seq.

(**D**) Expression distributions for *Myc*, *Top2a*, *Ctla4*, *Cd86*, *Pdcd1*, and *Cd274* at the single cell level in MM001i and MM008i tumors overlaid upon respective UMAPs.